

CERN Summer Student Report

Space Charge Effects in Simulations of Large Avalanche Dynamics

Abstract

An implementation of the space charge effect compatible with the microscopic tracking functionality of Garfield++ was created. The implementation used axisymmetric rings of charge, with the possibility of application to grid-free and grid-based simulations, depending on the speed and accuracy requirements. Two new classes were written, `ComponentChargedRing` for creating systems of charged rings and `ComponentGrid2D` for adding electric fields to the nodes of a 2D (r, z) grid and interpolating to points in between. Investigations were done into the granularity of the grid required for a satisfactory convergence of the field: convergence was found to be good for 20000 nodes/cm in each direction. Preliminary simulations were run in a parallel plate geometry: these showed significant field modifications and a gain limiting effect for 10^6 ionisations, whereas for 10^5 ionisations no such effects were observed. Support for resistive anodes were implemented, and the space charge electric field was found to be significantly modified when they were used.

Thomas Szwarczer

University of Oxford

30 June 2025 - 19 September 2025

1 Introduction

In gaseous detectors, incident ionising particles lead to charge deposition in a gaseous medium. These charges are accelerated by an electric field, leading to further ionisations, when the field is sufficiently strong. Alongside the applied electric field, an additional field due to the distribution of charges themselves exists within the medium. When this space charge field is comparable in magnitude to the background field, the behaviour of detectors may change: the so-called space charge effect commonly appears as a gain modification, and in extreme cases, streamer formation. A superexponential gain curve has been observed for resistive Micromegas detectors at gains $> 10^5$ [1], possibly a sign of this effect. Silicon detectors also show signs of the space charge effect, with a gain reduction being observed in LGADs for a larger number of initial charges [2].

Approaches to modelling the space charge effect can be divided into semi-analytic (where the fields of the charge configurations are calculated using analytic expressions and updated during the course of the simulation), finite element method approaches (see, for example, a hydrodynamical approach where the charge density is modelled as a ‘fluid’ coupled to the Poisson equation [3]) and neBEM approaches [4].

Simulations of large avalanche dynamics provide insights into the behaviour of electrons and ions in gaseous and silicon detectors. The Garfield++ toolkit [5] can be used to carry out detailed simulation of these avalanches in the presence of user-defined electric fields and detector geometries. Garfield++ allows for the microscopic simulation and collision-to-collision tracking of electrons through the class `AvalancheMicroscopic`; the space charge effect is currently unaccounted for in such simulations. In this project, contributions were made to Garfield++ to include this effect in microscopic simulations.

Two semi-analytic approaches were investigated. The first was the axisymmetric approximation, where the avalanche was modelled as a system of charged rings in free space, i.e. with no electrostatic boundary condition. The second was the point charge model, using point charge electric fields in a parallel plate boundary condition. The author’s contributions focused on the first of these. The new Garfield++ classes `ComponentChargedRing` and `ComponentGrid2D` were created and tested: electric field plots were made, and the gain-modifying effect was investigated. A comparison was made between the resulting electric fields from the two approaches: good agreement was found along the detector axis, except at the anode, where the interaction of mirror charges in the point charge case changes the field. Support for resistive anodes was implemented, and the space charge field was found to be significantly modified in comparison to the metallic anode case. Simulations were run with 10^5 and 10^6 ionisations, and a gain-modifying effect was confirmed for the latter case, reflecting the more significant modification of the field.

2 Methodology

2.1 Grid-based approaches

During the microscopic simulation of an electron, the local electric field will be requested by `AvalancheMicroscopic`. When this happens, the contribution to the space charge field from all relevant charges must be added up. For the axisymmetric approximation, the field of a charged ring might be re-calculated billions of times over the course of a simulation; even small operations, such as vector range-checking, add significant computation time. A possible approach to avoid such issues is to implement a grid in the simulation region, and calculate the electric field on the nodes only once for a given charge configuration. This process is outlined in Figure 1.

A grid can be used similarly in the point charge model. The analytic field of a point charge in a parallel plate involves a sum over a Bessel function, which is slow to compute, even if it is only done once per charge configuration. Under this model, further speedups can be made by snapping particles to the centre of grid cells (in order to avoid divergent fields on the nodes) and then loading pre-computed point charge fieldmaps, one for a point charge on each possible cell centre. Due to the parallel plate geometry, symmetry considerations were used to reduce the number of required fieldmaps to just one per node along the detector axis, saving memory.

Despite the performance improvements, there are disadvantages to using a grid. The first is that the process of interpolation results in a non-physical ‘splitting’ of the field, visible in Figure 2. Furthermore, for coarse grids in the axisymmetric approximation the field was observed to be a strong function of the grid spacing, and it was seen to converge well for grids of above 20000 nodes/cm in each direction (see Figure 3). This dependence on

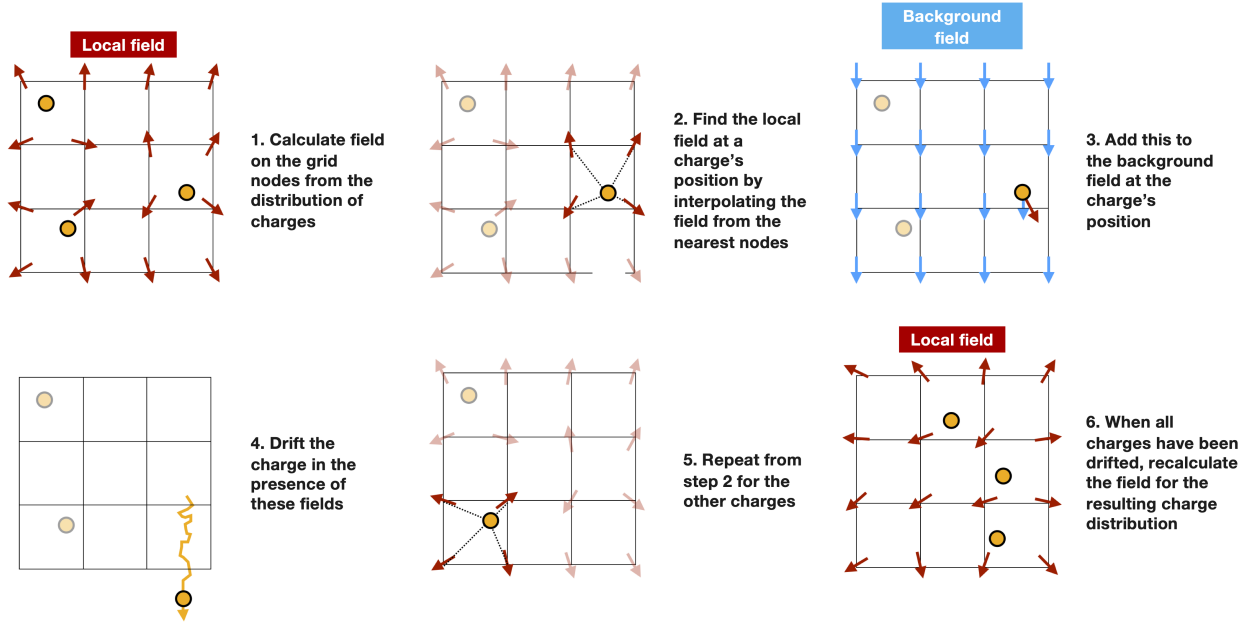


Figure 1: Description of the use of a grid in space charge simulations

grid spacing occurs because nodes close to divergent field regions necessarily sample higher field values, whereas divergences that lie close to the middle of two nodes are removed by the interpolation. The relative position of nodes changes with grid spacing for a constant volume of interest, causing the field to depend on the grid spacing.

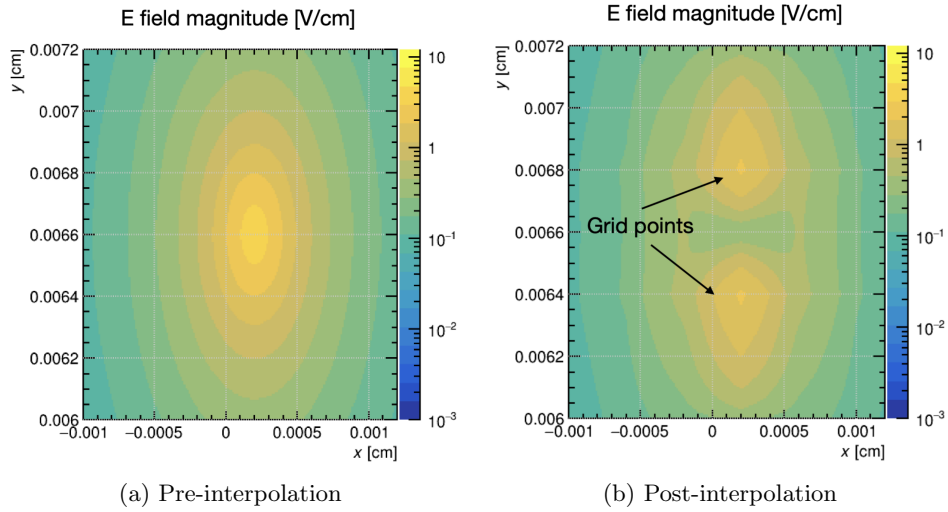


Figure 2: Splitting of the field due to interpolation. The field components E_x and E_z diverge to $\pm\infty$ in the vicinity of a ring. Hence, the interpolated value of these components passes through zero, leading to a sharp dip in the magnitude of the field at the location of the charge.

In order to avoid both of these issues, a grid-free approach was investigated for the axisymmetric approximation, and following significant optimisations, was found to be fast enough to justify its use over a grid-based approach, when there were less than 10^5 active electrons in the simulation. For higher numbers of active electrons, e.g. for applications with more than a single starting charge, the use of a grid was necessary.

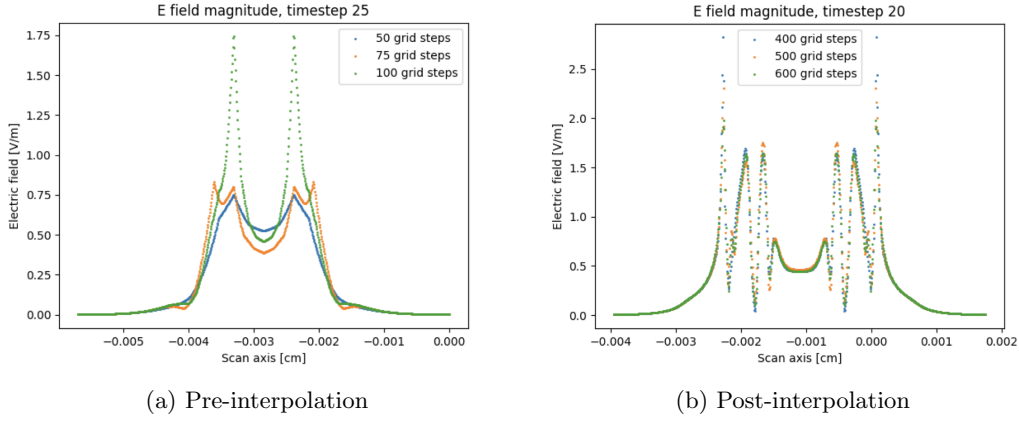


Figure 3: Comparison of the electric field, for a horizontal scan over multiple simultaneous grids. We see the field has a strong dependence on grid spacing for coarser grids. These plots come from different avalanches, at different points in their evolution.

2.2 Implementation of the axisymmetric approximation

2.2.1 ComponentChargedRing

The existing implementation of the space charge effect in Garfield++ was in the class `AvalancheGridSpaceCharge`, which is based on the work of C. Lippmann et al [6], and uses the axisymmetric approximation. In this class electrons are transported between grid nodes (on-grid transport), whereas in microscopic tracking they may drift arbitrarily (off-grid transport; note this is a different use of a grid to that of Section 2.1). A new class, `ComponentChargedRing`, was created so that the axisymmetric approximation could be used in both on- and off-grid transport of electrons. New functions were written to add rings to the simulation (including logic to remove rings of zero charge and merge nearby rings), update the symmetry axis dynamically and handle divergences if the field is called close to a ring. `ComponentChargedRing` does not itself use a grid, but its fields can be easily added to the nodes of a grid, e.g. using a `ComponentGrid` (for 3D grids) or `ComponentGrid2D` (for 2D grids) object.

Work was started to modify `AvalancheGridSpaceCharge` in order to use `ComponentChargedRing`, as well as update the example files, but was not completed before the end of the project.

2.2.2 ComponentGrid2D

The class `ComponentGrid` allows for the use of a 3D grid, meaning that for an application with symmetry, more calculations are done than are necessary. It was found that a `ComponentGrid` simulation was not faster than a grid-free simulation for fewer than about 10^6 active electrons. This motivated the creation of a new class, `ComponentGrid2D`, for working with an (r, z) grid in applications with cylindrical symmetry. This class built on the grid implementation from `AvalancheGridSpaceCharge`, with a new function added to interpolate the field from the nearest nodes.

2.2.3 Tolerances and divergence handling

The axisymmetric approach has two user-defined positional tolerances:

- The tolerance below which two rings are counted as identical, and the charge of one is added to the other (ring spacing tolerance). This value acts to limit the number of active rings in the simulation, and can be used to reduce computation time.
- The tolerance between a field evaluation point and a ring position below which the divergence must be dealt with (self-field tolerance). Details of how divergences are handled can be found below.

It should be noted that point charges were created on the symmetry axis when the radius of the associated ring was less than a unit of ring spacing tolerance, in order to avoid a single ‘smallest ring’ with a significant amount of charge assigned to it.

If divergences are not dealt with, electrons may cross regions of infinite field, and the first electron in the simulation will feel an infinite self-field. The approach taken to prevent this was, in the case of a field value being requested within one self-field tolerance of a ring, to instead calculate the field at one self-field tolerance away from the divergent point. This value is then assigned to the point of interest. An efficient check of the relative position of the ring and field point allowed for the sign of the field to be preserved while the divergence was mitigated. If the field was requested exactly on the position of a ring, field values of 0 were returned: this was relevant for the first electron in the simulation.

2.2.4 Structure of the simulation

An example program to simulate an avalanche using the space charge effect with microscopic tracking was added to Garfield++ (`MicroscopicSpaceCharge.C`). An outline of the simulation can be seen in Figure 4. An adaptive time window was implemented, in order to keep the amplification factor over a time window roughly constant; more details can be found in Section 3.1.

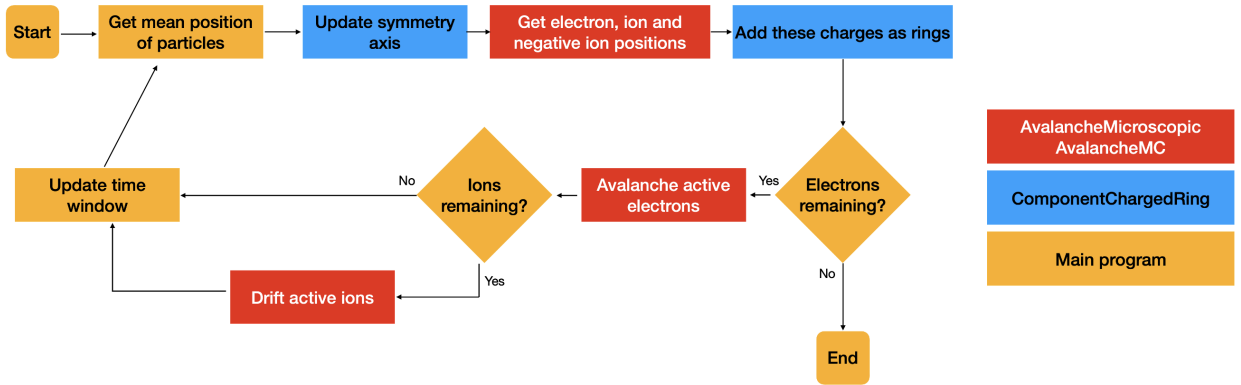


Figure 4: Flow diagram showing the basic functionality of the simulation program

2.2.5 Visualising the field

Plots of the space charge electric field were produced. The low field in the central region was explained by the E_x, E_z components switching polarity around the axis of symmetry, as seen in Figure 5.

Plots of field close to the symmetry axis¹ were produced, shown in Figure 6.

2.2.6 Effect of a resistive anode

Plots of the field close to the axis following simulations with and without a resistive anode condition were done. The resistive condition was implemented by using two `ComponentChargedRing` objects; one for the bulk of the avalanche and one for electrons ‘stuck’ on the anode. The use of two separate `ComponentChargedRing` objects allowed the field from electrons at the anode to be treated independently of the main ring system field, and thus allowed them to be compared; the results of this comparison can be seen in Figure 7.

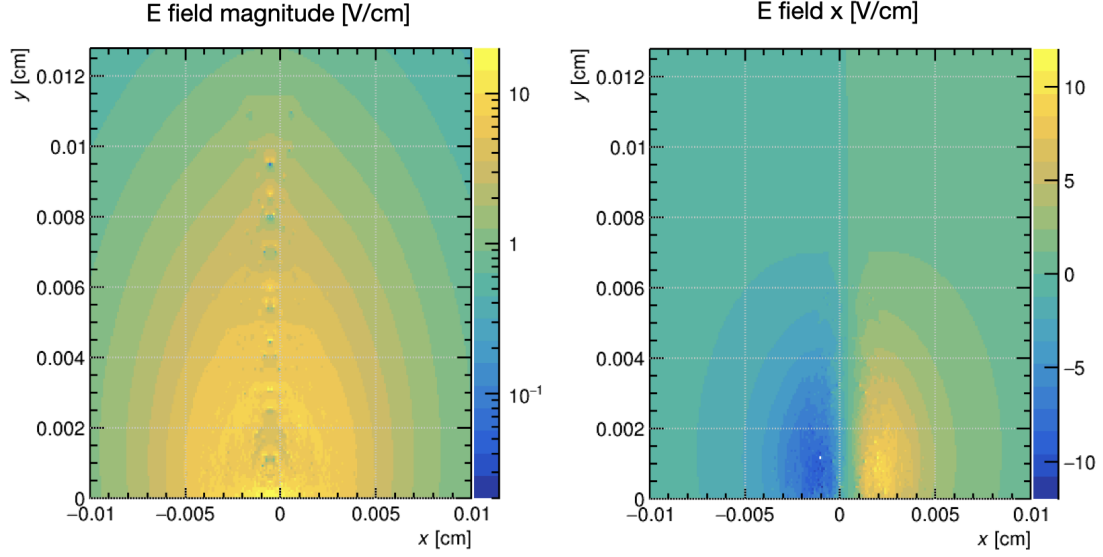


Figure 5: Reference electric field plots. Note that a grid was not used for these plots, and that they were done with few electrons active in the simulation; hence there is no smoothing due to interpolation, and discontinuities due to the rings are more visible. Note further that the background electric field was not included in these plots.

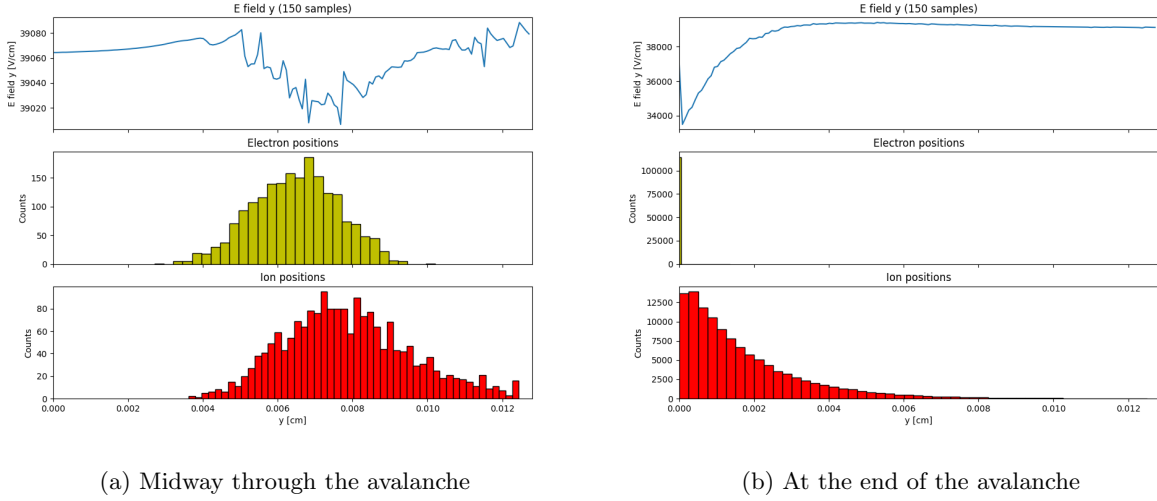


Figure 6: Electric field magnitude, and electron (yellow) and ion (red) occupation for scans slightly offset from the symmetry axis. Note that a resistive anode was used in these plots.

2.2.7 Charge densities required to significantly modify the applied field

Figure 8 shows that the field modification due to the space charge is not very significant at 1.6×10^5 ionisations, but is reduced by up to half at 1.5×10^6 ionisations.

2.2.8 Profiling

Extensive profiling was done using the tool Callgrind [7]. A line-by-line analysis of the existing and new functions was done, revealing bottlenecks in the functions that retrieve elliptic integral values and calculate the electric field. Significant optimisations were made by avoiding unnecessary range checking and reducing the number of computationally expensive operations to be done when calculating the field of a charged ring.

¹The field could not be evaluated directly along the symmetry axis, as the point charges present there produced high fields that dominated the plots. See Section 2.2.3 for more details.

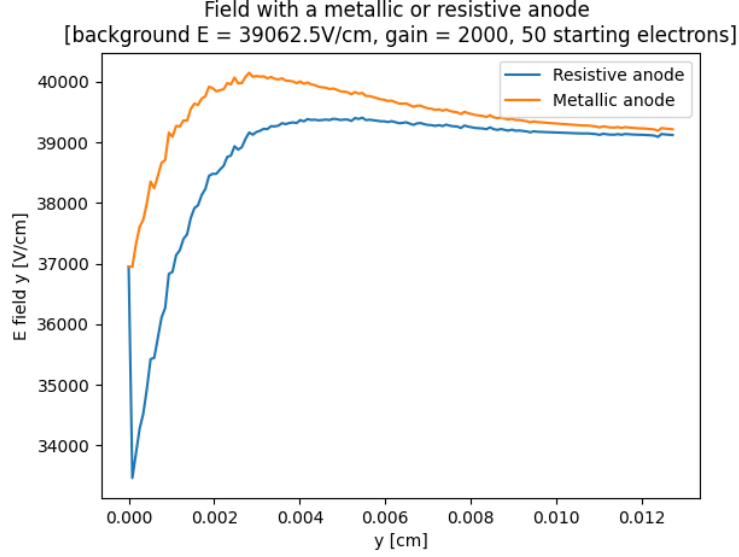


Figure 7: The field was found to be significantly modified when a resistive anode was used compared to a metallic one. The plot shows the space charge field at the end of the avalanche, when all electrons have been collected on the anode. The background field is included.

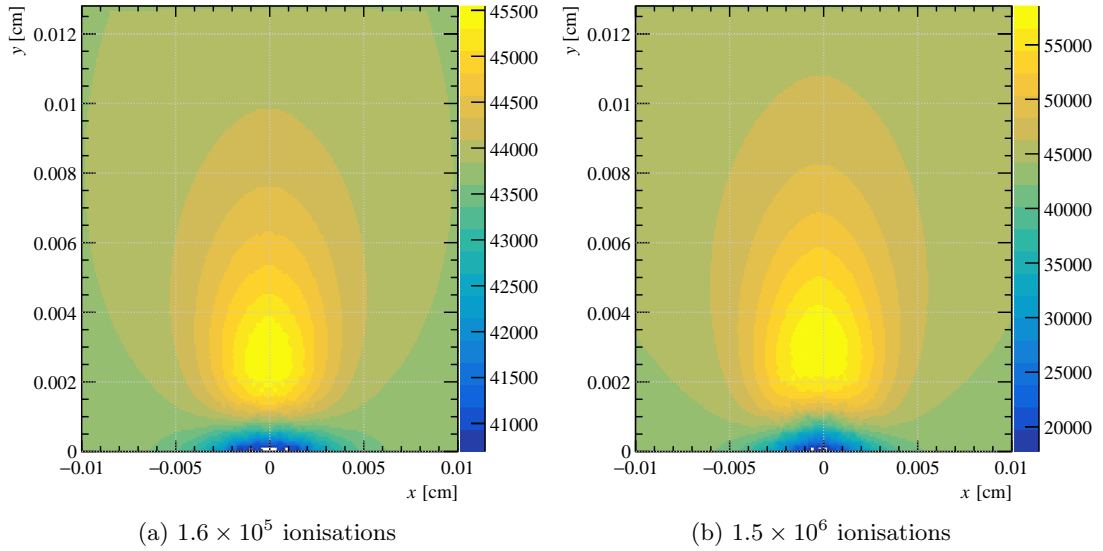


Figure 8: The modification of the electric field becomes significant at 10^6 ionisations. Note that the background field was the same in these two plots, at 43,750V/cm, and is included in the plots. Note further that the white area at the bottom of the plots is an artefact of plotting; it was verified that the space charge field was well-behaved in this region. The plots show the field magnitude with units of V/cm.

2.3 Point charge approach

Investigations were done² into using the fields of point charges directly instead of approximating the avalanche as axisymmetric. The point charges were placed within a parallel plate geometry, meaning the resulting field involved contributions from an infinite number of mirror charges. The analytic expression for this field includes a slowly-converging sum over a Bessel function, which was computationally intensive to evaluate in real time during a simulation. In order to improve performance, fieldmaps were pre-computed as detailed in Section 2.1. A 3D grid was used, in comparison to the 2D grid of the axisymmetric approximation. The use of fine grids was limited by the large file sizes of the fieldmaps, and the computation cost of evaluating the field on many grid nodes, although the former was partially mitigated by exploiting the horizontal symmetry of a point charge in an infinite parallel plate.

²This work was undertaken by the supervisor of this project, Djunes Janssens.

2.3.1 Comparison between axisymmetric and point charge approaches

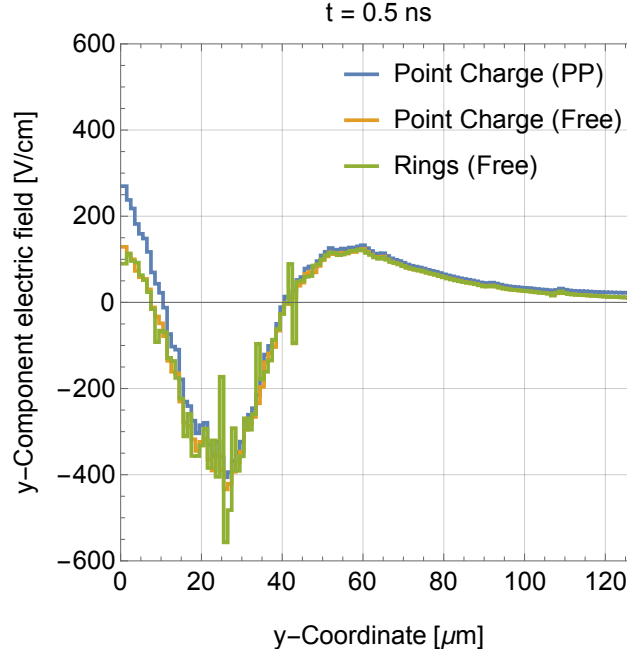


Figure 9: Comparison between the fields of point charges in a parallel plate boundary condition (labelled “PP”), point charges in free space and charged rings in free space.

There was good agreement between the space charge field under the axisymmetric approximation and the point charge approach; the field with and without the parallel plate boundary condition was also compared. The results can be seen in Figure 9. It is worth noting the presence of spikes in the axisymmetric field. These are present because the field was scanned along the symmetry axis, meaning the divergent fields due to the point charges present on this axis were sampled (see Section 2.2.3). Also of note is the deviation between the two free space models and the model with the parallel plate boundary condition at the anode. This field modification was due to the presence of mirror ions.

3 Results

The gas mixture used in these simulations was Argon/CO₂ (93/7), at atmospheric pressure and at 293.15K.

3.1 Effect of time window size on gain

As the number of rings present in the simulation is updated at the end of each time window, for longer time windows there will be more charges unaccounted for, especially when the charges are undergoing high levels of amplification. An adaptive time window length was implemented in the example file `MicroscopicSpaceCharge.C`; if a large amount of amplification occurred over a time window, the time window was reduced in order to limit many charges being unaccounted for. In this way, a maximum allowed limit on the amplification over a time window could be set.

A preliminary simulation showed an unexpected gain reduction at gains of 10^3 , where we would not expect any significant space charge effects. This motivated an investigation into the gain difference between simulations with space charge enabled and disabled, at low gains, as the allowed limit of missed charge was varied. The results (see Figure 10) showed only statistical fluctuations, revealing no clear evidence of a gain discrepancy at low gains, regardless of the missed charge percentage.

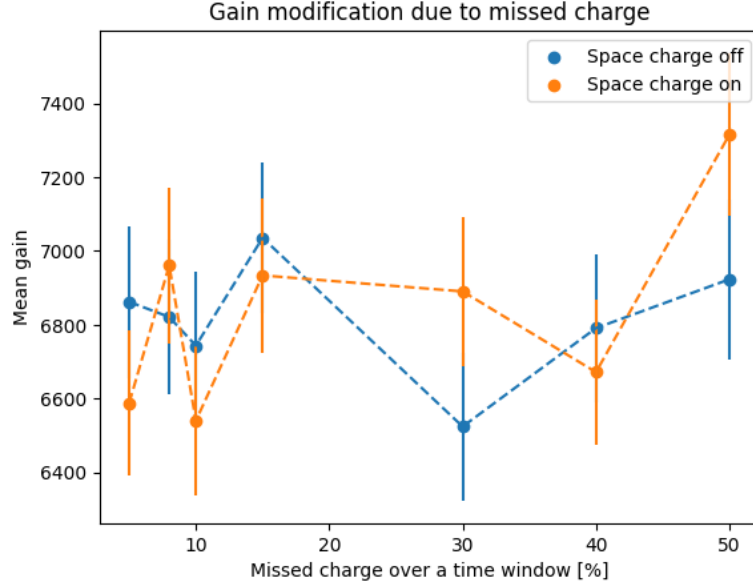


Figure 10: Results of varying the maximum allowed percentage change in charge over a time window. A missed charge percentage of, say, 20% means that the number of charges present in the simulation can change by a maximum of 20% over a time window.

3.2 Preliminary high-gain simulations

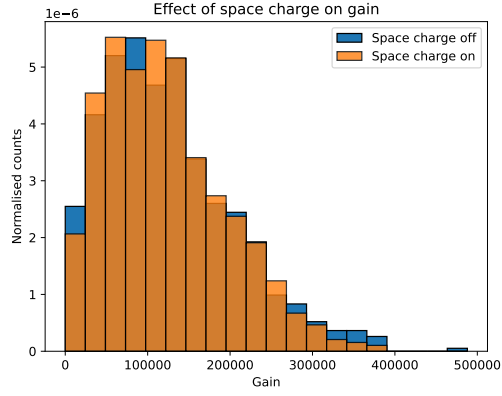
Investigations were done into the effect of space charge on gain at a mean gain of 10^5 , motivated by the superexponential behaviour observed to occur in Micromegas detectors at around this value. The simulations were done in a parallel plate of size $128\mu\text{m}$, voltage 660V, with a single primary electron being added at a height of $127.9\mu\text{m}$. The parallel plate was used as it is easy to implement in Garfield++, resembles the amplification stage of a Micromegas, and has analytic expressions for the fields of charges within it, although these simulations used charged rings in free space. A fixed time window of 2.5ps was used, and the anode was modelled as metallic, i.e. electrons reaching it were evacuated. The resulting gain spectra can be seen in Figure 11a.

A two-tailed permutation test of 10^4 permutations was done on the results, yielding no significant difference in gain with space charge at a p -value of 5%. Nevertheless, a potential sign of gain-limiting behaviour could be seen in the tail of the distribution, which motivated investigations with more active electrons.

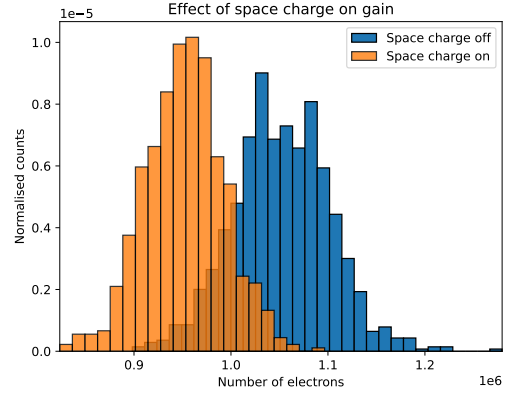
Further simulations were run, aiming for a higher number of simulated charges, to create an environment of significant field modification. 200 starting charges were used, in the previous parallel plate geometry, under a voltage of 540V. The results, shown in Figure 11b, show a clear gain limiting effect due to the space charge field.

4 Conclusion

Contributions were made to Garfield++ in order to take the space charge effect into account in microscopic tracking simulations. The class `ComponentChargedRing` was written, which allows for the space charge field of an avalanche with cylindrical symmetry to be modelled, with the possibility of using a grid (implemented with the class `ComponentGrid2D`) to reduce computation time. When a coarse grid was used, the space charge field was found to be a strong function of the grid spacing. The effect of a resistive anode was investigated, and was found to significantly reduce the field at the end of the avalanche. A gain-limiting effect was observed in a parallel plate geometry as a result of the space charge modifying the applied field. Good agreement was found between axisymmetric and point charge approaches, except at the anode, where mirror charge effects became important.



(a) One starting electron, 660V



(b) 200 starting electrons, 540V

Figure 11: Gain spectra. For a larger number of charges in the simulation, the field is significantly modified, leading to a visible gain-limiting effect

Acknowledgements

I would like to thank my supervisors, Djunes Janssens and Heinrich Schindler, for their guidance during this project, and for giving me the opportunity to undertake this work. I would also like to thank the CERN GDD group: it was a pleasure to work with you all!

References

- [1] Jianxin Feng et al. “A thermal bonding method for manufacturing Micromegas detectors”. In: *Nuclear Instruments and Methods in Physics Research Section A: Accelerators, Spectrometers, Detectors and Associated Equipment* 989 (2021), p. 164958. ISSN: 0168-9002. DOI: <https://doi.org/10.1016/j.nima.2020.164958>.
- [2] E. Currás, M. Fernández, and M. Moll. “Gain reduction mechanism observed in Low Gain Avalanche Diodes”. In: *Nuclear Instruments and Methods in Physics Research Section A: Accelerators, Spectrometers, Detectors and Associated Equipment* 1031 (2022), p. 166530. ISSN: 0168-9002. DOI: <https://doi.org/10.1016/j.nima.2022.166530>.
- [3] Purba Bhattacharya et al. “Numerical simulation of charging up, accumulation of space charge and formation of discharge”. In: *Nuclear Instruments and Methods in Physics Research Section A: Accelerators, Spectrometers, Detectors and Associated Equipment* 1075 (2025), p. 170336. ISSN: 0168-9002. DOI: <https://doi.org/10.1016/j.nima.2025.170336>.
- [4] Tanay Dey et al. “Parallelization of Garfield++ and neBEM to simulate space-charge effects in RPCs”. In: *Computer Physics Communications* 294 (2024), p. 108944. ISSN: 0010-4655. DOI: <https://doi.org/10.1016/j.cpc.2023.108944>. URL: <https://www.sciencedirect.com/science/article/pii/S0010465523002898>.
- [5] URL: <https://garfieldpp.web.cern.ch/>.
- [6] C Lippmann and W Riegler. “Space charge effects in Resistive Plate Chambers”. In: *Nuclear Instruments and Methods in Physics Research A*, vol. 517, p.54 (2004).
- [7] URL: <https://valgrind.org/docs/manual/cl-manual.html>.